



An Investigation on Flow Structure and Heat Transfer Characteristics of Confined Impinging Twin Jets

Yücel ÖZMEN¹ and Haluk KELEŞ²

How to cite: Özmen, Y., & Keleş, H. (2023). An investigation on flow structure and heat transfer characteristics of confined impinging twin jets. *Sinop Üniversitesi Fen Bilimleri Dergisi*, 8(2), 178-201. <https://doi.org/10.33484/sinopfbid.1365843>

Research Article

Corresponding Author

Yücel ÖZMEN
yozmen@ktu.edu.tr

ORCID of the Authors

Y.Ö.: 0000-0003-1127-1060
H.K.: 0000-0002-6562-8902

Received: 25.09.2023

Accepted: 20.11.2023

Abstract

An investigation into the heat transfer performance and flow characteristics of circular twin jets was conducted using both numerical and experimental methods. The jets emanated from the lower surface and were confined to impinge perpendicularly on the upper surface. To simulate the bidimensional impinging twin jet flow field with powerful turbulence and heat transfer, Realizable $k-\epsilon$ and Standard $k-\omega$ turbulence models were employed. Reynolds numbers ranging from 30000 to 50000 were used in both simulations and experiments, with jet-to-jet spacing ranging from 0.5 to 2 and nozzles to target impingement plate spacing in the same range. Sub-atmospheric pressure regions were detected on the impingement surface in experimental measurements for spacing up to 1, whereas numerical results suggested that they could be found at all nozzle to target impingement plate spacings studied. A correlation was discovered between the peaks in coefficients of heat transfer on the target surface and the sub-atmospheric regions in pressure distributions.

Keywords: Twin impinging jet, sub-atmospheric region, turbulence models, pressure coefficient, Nusselt distribution

Sınırlandırılmış Çarpan İkiz Jetlerin Akış Yapısı ve Isı Transferi Karakteristikleri Üzerine Bir İnceleme

¹Karadeniz Technical University,
Department of Mechanical
Engineering, Trabzon, Türkiye

²Artvin Çoruh University,
Department of Electrical and
Electronics Engineering, Artvin,
Türkiye

This work is licensed under a
Creative Commons Attribution
4.0 International License

Öz

Sayısal ve deneysel yöntemler kullanılarak dairesel ikiz jetlerin ısı transferi performansı ve akış karakteristikleri üzerine bir araştırma gerçekleştirildi. Jetler alt yüzeyden yayılmış ve üst yüzeye dik olarak çarpmak üzere sınırlandırılmıştır. İki boyutlu çarpan ikiz jet akış alanındaki güçlü türbülans yapılarını ve ısı transferini simüle etmek için Realizable $k-\epsilon$ ve Standard $k-\omega$ türbülans modelleri kullanılmıştır. Hem simülasyonlarda hem de deneylerde 30000 ila 50000 arasında değişen Reynolds sayıları kullanılmış, jetler arası mesafe 0.5 ila 2 arasında değişmiş ve lüleler ile hedef çarpma levhası arası mesafe de aynı aralıkta olmuştur. Deneysel ölçümlerde açıklığın 1'e kadar olduğu durumlar için hedef çarpma yüzeyinde atmosfer altı basınç bölgeleri tespit edilirken, sayısal sonuçlar bunların incelenen tüm lüle hedef levha aralıklarında bulunabileceğini göstermiştir. Hedef yüzeydeki ısı transferi katsayılarındaki tepe noktaları ile basınç dağılımlarındaki atmosfer altı bölgeler arasında bir korelasyon keşfedilmiştir.

Anahtar Kelimeler: İkiz çarpan jet, sub-atmosferik bölge, türbülans modelleri, basınç katsayısı, Nusselt dağılımı

Introduction

The highly attractive rate of local heat and mass transfer performance of single or multi-array impinging jets have made them a popular choice for a wide array of industrial applications. Jet impingement finds applications in a variety of industries, such as glass shaping and tempering, fabric and cardboard drying, airfoil deicing, turbine blade and computer electronics cooling. In the last three decades, the investigation of flow fields and structures as well as heat transfer performance via single or multiple jets impingement has remained an energetic area of research, with both numerical and experimental studies being conducted. While high heat transfer coefficients are offered by impinging single jets in the stagnation zone, the performance of cooling decreases dramatically beyond the impinging zone. In the cooling process carried out with multiple jets, a single jet can be used or multiple jets can be used simultaneously. While the use of a single jet increases the heat transfer in a certain region, the use of multiple jets makes the distribution of heat transfer more homogenous on the surface to be cooled. In consequence, impinging jets are often favoured in arrays in a variety of applications. In such cases, effective temperature reduction heavily relies on the interplay among the jets within the array. There are many studies and applications in the literature that pay attention to the characteristics of flow structure and performance of heat and mass transfer in jet impingement of twin patterns. In most of these studies, the flow is laminar character. Studies on turbulent impinging multi-jets are very few. The studies on this subject are mostly in the form of numerical analyses. In a study they conducted, Barata et al. [1] investigated the turbulent jets impingement of single and twin types with confining plates through a cross flow and observed that both configurations had a similar pattern with significant jet penetration. Chuang et al. [2] utilized a bidimensional (2D) mathematical model to examine compressible and unsteady flow properties of twin-slot jet impingement amid two plates. In their research, Chuang and Nieh [3] utilized the PHOENICS code to explore impinging square twin jets flow's three-dimensional (3D) turbulent structure without cross flow. In their comprehensive literature review, Polat et al. [4] noted that the Standard k- ϵ model with miscellaneous wall functions is inadequate for accurately predicting stagnation heat transfer and suggested that k- ϵ models with low Reynolds number and strong streamline curvature pose a challenge for testing advanced turbulent models in jet impingement flows, pressure gradient, and recirculating zones. In their study, Shi et al. [5] examined the influence of turbulence models, turbulence intensity, Reynolds number (Re), close wall applications, and boundary conditions in a slot jet for heat transfer. The study utilized both the Standard k- ϵ and Reynolds Stress (RSM) models. To simulate turbulent flow and analyze heat transfer performance from confined multi-array slot jets impingement in a 2D environment, Seyedein et al. [6] utilized a mathematical technique. Dianat et al. [7] utilized the Standard k- ϵ turbulence model to foresee the behavior of nonsymmetric and bidimensional impinging turbulent jets. Numerical analysis was carried out by Fernandez et al. [8] to study the turbulence flow behavior of an impinging twin-plane jet perpendicularly on a flat surface. The study employed both Realizable and Standard k- ϵ and Standard k- ω turbulence models. According to

the researchers' conclusion, these models failed to provide an accurate prediction of the flow in the zone of the impact. Miao et al. [9] examined the structure and characteristics of the fluid flow and heat transfer performance of a confined circular jet array orthogonal to a flat plate, at various cross-flow orientations. Distributions of Nusselt number figured out by them overall on the flat plate. In their study, Qui et al. [10] developed a numerical model for a 2D configuration an opposed jet to investigate the flow characteristics and blending performance of opposed laminar jet flows. Attalla and Specht [11] conducted an experimental study on convective heat transfer performance on a flat plate using a multi-jet system. The study concluded that, they observed that the use of a multi-array jet system leads to an increase in both local and mean heat transfer rates compared to a single nozzle. Aldabbagh and Mohamad [12] numerically analyzed the effects of jet to target impingement plate spacing in an impinging laminar square jet array confined with a plate. A numerical study was conducted by Dagtekin and Oztop [13] to investigate the impact of distance from floor to wall, Reynolds number and distance of jet-to-jet for two jets on fluid flow structure, characteristics and heat transfer performance. In the impingement of twin square laminar jets, the performance of heat transfer and also structure of fluid flow were investigated numerically by Aldabbagh and Sezai [14]. According to the obtained outcomes, the flow pattern of impinging twin square jets on a preheated target surface was significantly influenced by the distance between the jets and the target impingement plate, as reported by the study conducted by them. The interplay between the boundary layer of the wall jet and the free shear layer was studied experimentally by Ho and Hsiao [15] using a specific technique. By utilizing an experimental approach, Siclari et al. [16] studied the formation of upwash and stagnation lines in two impinging jets. Tanaka [17] observed a unique characteristic in the twin jet's 2D parallel flow, which was the formation of a region of sub-atmospheric pressure amid the jets due to the turbulent fluid flow entrainment. Abdel-Fattah [18] reported that a region of sub-atmospheric pressure appeared on the impingement surface in the impinging twin round jet flow, and this effect decreased as the nozzle to target impingement plate spacing increased. Mikhail et al. [19] explained that as the jet-to-jet spacing decreases, the average Nusselt number of a twin jet system increases. Barata [20] conducted laser doppler measurements to investigate structures, fields and characteristics of the flow generated by impinging twin jets on a ground plane. The results of the study revealed the presence of a complicated 3D scarf vortex that forms round about the impinging jets. An experimental investigation conducted by Dong et al. [21] on the heat transfer performance and wall pressure features of a vertical laminar twin air jet impinging on a horizontal flat plate. Their study aimed to interpret the impact of the twin jets on heat transfer and pressure distribution by examining their interactions with the plate's surface. An experimental investigation was carried out by Saad et al. [22] on the flow structure and heat transfer performance of impinging confined single and multi-slot jet flows. They stated that multiple jets exhibit single jet characteristics at values of 1.5 and higher than the nozzle spacing ratio. Özmen [23] experimentally investigated the flow fields and structures for a confined twin air jet impinging on a flat surface. He

determined that sub-ambient pressure regions are formed on both the impingement and confining surface and that the pressure distributions on the surfaces are influenced by the nozzle to target impingement plate spacing and the distance of nozzle to nozzle. Buchlin [24], in his study of impinging array jet flow, stated that nozzle to target impingement plate and nozzle to nozzle distances have a direct effect on jet characteristics. Polat et al. [25] carried out a comprehensive literature survey on heat transfer in impinging jet flows, including both experimental and numerical studies. They pointed out that low Reynolds number $k-\varepsilon$ turbulence models, which are among the turbulence models used in numerical studies, predict the heat transfer at the stagnation point more accurately than the Standard $k-\varepsilon$ turbulence model. Özmen and İpek [26] experimentally and numerically investigated the flow fields and structures furthermore heat transfer performance of jet flow generated by multiple slot jets impinging on a target flat surface. They highlighted that there is a significant correlation between the sub-ambient pressure regions formed on the impingement surface and the secondary peaks in the Nusselt distributions. Özmen and Baydar [27] numerically investigated the flow fields and structure furthermore heat transfer performance of confined jet array flow impinging on a surface. They stated that both pressure distributions and Nusselt distributions throughout the target impingement surface are significantly influenced by the nozzle to target impingement plate spacing. Afroz and Sharif [28] numerically analyzed the cooling of a constant temperature surface by an inclined impinging twin slot jet using different jet-target impingement plate distances, Reynolds numbers and turbulence models. Yousefi-Lafouraki et al. [29] numerically modelled and investigated effects of the flow and heat transfer in their study where both the impingement plate and the confining plate are inclined. The study carried out at low inclination angles showed that the mean Nusselt number increases with increasing inclination angle. Al-Rmah and Mohamad [30] with six-in-line jet outlets different channel heights and nozzles in a double-pass channel effects of widths on heat transfer and flow structure Reynolds number numerically in the range of 100 to 400 analyzed. Guongeng et al. [31] experimentally observed the effects of different values of jet-cross-flow velocity ratios and different channel heights on the local and mean. Nusselt numbers for a flow region subjected to cross-flow with a series of sequential jets. Lam and Prakash [32] investigated two-dimensional and numerical refrigeration of split heat sources by a pair of air jets for duct heights and velocity ratios of the jets; they analyzed in detail the effects of the relevant parameters on the local and mean Nusselt number variation and entropy production and determined the optimum velocity ratios. Paulraj et al. [33] numerically investigated the effects of duct height and distance between blocks on convection heat transfer in cooling of discrete blocks with constant surface temperature by slot jets in the range of Reynolds number between 30 and 300, focusing on the velocity profiles around the blocks and the variation of local and mean Nusselt numbers on the surfaces of the blocks. Kaya [34] numerically investigated the effect of surface shape (flat, zigzag, rectangular, trapezoidal) on convection heat transfer from a heated target impingement plate cooled by a pair of circular jets and determined that convection heat transfer characteristics are significantly influenced by

surface shape. Martinez-Filgueira et al. [35] investigated the effects of the fluid exiting from different nozzles on the wall shear stress and heat transfer in the cooling process performed with multiple impinging jets; they compared the effects of different turbulence models on the results. Demircan and Türkoğlu [36], numerically investigated the effects of oscillation characteristics on the flow structure and heat transfer performance in an impinging slot jet and stated that jet oscillation has no influence on the stagnation Nusselt number for $H/W < 1.5$. Bölek and Bayraktar [37] numerically carried out on the flow structure and heat transfer performance of a jet impinging on different types of impact surfaces. Çalışır et al. [38] numerically examined the flow structures of a series of circular impinging air jets on triangular and square ribbed surfaces. Several investigations [2, 39-44] on impinging single and twin jet flows have reported satisfactory consistency between numerical predictions and experimental results. The flow field resulting from jet impingement on a target impingement plate surface, as well as the wall jet flow developed downstream between twin jets, are highly complex phenomena. This study aims to investigate the flow fields of confined impinging twin jets employing both experimental and numerical techniques. In this current study, the influence of multifarious jet flow specifications, such as spacings of jet-to-jet and nozzle to target impingement plate, on the flow features of impinging twin jets confined with plate were experimentally and numerically examined. The examined flow parameters included pressure distribution of surface, Nusselt distribution, turbulence intensity and axial mean velocity. The experiments were conducted at Reynolds numbers of 30000, 40000, and 50000, while the spacings of nozzle to target impingement plate were set to 0.5, 1, and 2, and the distance between jets were set to 0.5, 1, and 2 as well. The major objective of this investigation is to evaluate the effectiveness of assorted turbulence models in forecasting the heat transfer performance and flow features of confined impinging twin-jets configurations by contrasting them with the experimental results obtained in the present study. The second goal of the study is to establish a connection between the flow characteristics of the confined impinging twin jets and the corresponding heat transfer distributions. It is anticipated that the results and outcomes of this study will provide valuable data for further investigations in this field.

Materials and Methods

Numerical Study

Mathematical Model

In this study, a steady state, turbulent and Newtonian air flow with bank on temperature fluid features was assumed. To obtain a mathematical solution for the mean flow and thermal fields, it is required to solve the Reynolds Average Navier-Stokes (RANS) equations and the time-averaged energy equations. Below is the form of these equations, written for 2D incompressible flow in cylindrical coordinates with the continuity equation included, mass continuity:

$$\frac{\partial}{\partial z}(\rho u) + \frac{1}{r} \frac{\partial}{\partial r}(r \rho v) = 0 \tag{1}$$

z-momentum

$$\frac{\partial}{\partial z}(\rho u u) + \frac{1}{r} \frac{\partial}{\partial r}(r \rho v u) = -\frac{\partial p}{\partial z} + \frac{\partial}{\partial z} \left(\mu_{eff} \frac{\partial u}{\partial z} \right) + \frac{1}{r} \frac{\partial}{\partial r} \left(r \mu_{eff} \frac{\partial u}{\partial r} \right) + S^u \tag{2}$$

r-momentum:

$$\frac{\partial}{\partial z}(\rho u v) + \frac{1}{r} \frac{\partial}{\partial r}(r \rho v v) = -\frac{\partial p}{\partial r} + \frac{\partial}{\partial z} \left(\mu_{eff} \frac{\partial v}{\partial z} \right) + \frac{1}{r} \frac{\partial}{\partial r} \left(r \mu_{eff} \frac{\partial v}{\partial r} \right) + S^v \tag{3}$$

energy:

$$\rho C_p \left(u \frac{\partial T}{\partial z} + v \frac{\partial T}{\partial r} \right) = k \left[\left(\frac{\partial^2 T}{\partial z^2} \right) + \left(\frac{1}{r} \frac{\partial}{\partial r} \left(r \frac{\partial T}{\partial r} \right) \right) \right] + \mu \Phi \tag{4}$$

The origin terms (S^u and S^v) and the viscous loss function (Φ) in the equations can be expressed by the following formulas.

$$S^u = \frac{\partial}{\partial z} \left(\mu_{eff} \frac{\partial u}{\partial z} \right) + \frac{1}{r} \frac{\partial}{\partial r} \left(\mu_{eff} r \frac{\partial v}{\partial z} \right) \tag{5}$$

$$S^v = \frac{\partial}{\partial z} \left(\mu_{eff} \frac{\partial u}{\partial r} \right) + \frac{1}{r} \frac{\partial}{\partial r} \left(\mu_{eff} r \frac{\partial v}{\partial r} \right) - 2 \mu_{eff} \frac{v}{r^2} \tag{6}$$

$$\Phi = \left\{ 2 \left[\left(\frac{\partial v}{\partial r} \right)^2 + \left(\frac{v}{r} \right)^2 + \left(\frac{\partial u}{\partial z} \right)^2 \right] + \left(\frac{\partial v}{\partial z} + \frac{\partial u}{\partial r} \right)^2 - \frac{2}{3} (\nabla \cdot V)^2 \right\} \tag{7}$$

Mathematical solutions were performed using both the Realizable k-ε and Standard k-ω turbulence models. Two equation turbulence models utilize the Boussinesq close resemblance to establish a relationship between the stresses of Reynolds and the average velocity gradients. The Realizable k-ε model attempts to address some of the limitations of traditional k-ε models by incorporating the physical nature of turbulent flows into the calculation of normal stress, thereby reducing some of the mathematical constraints. The Realizable k-ε model calculates the turbulent kinetic energy [k (m²/s²)] and rate of dissipation [ε (m²/s³)] using the following equations:

turbulence kinetic energy (k):

$$\frac{\partial}{\partial z}(\rho u k) + \frac{1}{r} \frac{\partial}{\partial r}(r \rho v k) = \frac{\partial}{\partial z} \left(\Gamma_k \frac{\partial k}{\partial z} \right) + \frac{1}{r} \frac{\partial}{\partial r} \left(r \Gamma_k \frac{\partial k}{\partial r} \right) + S^k \tag{8}$$

turbulence dissipation rate (ε):

$$\frac{\partial}{\partial z}(\rho u \varepsilon) + \frac{1}{r} \frac{\partial}{\partial r}(r \rho v \varepsilon) = \frac{\partial}{\partial z} \left(\Gamma_\varepsilon \frac{\partial \varepsilon}{\partial z} \right) + \frac{1}{r} \frac{\partial}{\partial r} \left(r \Gamma_\varepsilon \frac{\partial \varepsilon}{\partial r} \right) + S^\varepsilon \tag{9}$$

In the foregoing equations, the radial (r) and axial (z) velocity vector elements are represented as u and v , fluid density symbolize with ρ , and the effective viscosity is μ_{eff} for momentum transport given as below

$$\mu_{eff} = \mu + \mu_t \tag{10}$$

The molecular viscosity, μ , and the "turbulent" viscosity, μ_t , are related through the following expression:

$$\mu_t = C_\mu \rho k^2 / \varepsilon \tag{11}$$

The exchange coefficients that account for the effects of turbulence on the transport of turbulent kinetic energy [k] (m^2/s^2) and rate of dissipation (ε) are expressed by the following equations

$$\Gamma_k = \mu + \frac{\mu_t}{\sigma_k} \tag{12}$$

$$\Gamma_\varepsilon = \mu + \frac{\mu_t}{\sigma_\varepsilon} \tag{13}$$

Where σ_k and σ_ε are the turbulent Prandtl/Schmidt numbers. S^k and S^ε perform source terms for k and ε . The following expressions provide them

$$S^k = \mu_t \left[2 \left\{ \left(\frac{\partial u}{\partial z} \right)^2 + \left(\frac{\partial v}{\partial r} \right)^2 + \left(\frac{v}{r} \right)^2 \right\} + \left\{ \frac{\partial v}{\partial z} + \frac{\partial u}{\partial r} \right\}^2 \right] - \rho \varepsilon \tag{14}$$

$$S^\varepsilon = C_1 \frac{\varepsilon}{k} \mu_t \left[2 \left\{ \left(\frac{\partial u}{\partial z} \right)^2 + \left(\frac{\partial v}{\partial r} \right)^2 + \left(\frac{v}{r} \right)^2 \right\} + \left\{ \frac{\partial v}{\partial z} + \frac{\partial u}{\partial r} \right\}^2 \right] - C_2 \rho \frac{\varepsilon^2}{k} \tag{15}$$

Constant are employed with standard values: $C_1=1.44$, $C_2=1.9$, $C_\mu = 0.09$, $\sigma_k = 1.0$, $\sigma_\varepsilon = 1.2$. The Standard $k-\omega$ model is a turbulence model that utilizes transport equations for turbulent kinetic energy (k) and rate of specific dissipation [$\omega=\varepsilon/k$] ($1/s$). The transport equations for k and ω are given as follows:

$$\frac{\partial}{\partial z}(\rho u k) + \frac{1}{r} \frac{\partial}{\partial r}(r \rho v k) = \frac{\partial}{\partial z} \left(\Gamma_k \frac{\partial k}{\partial z} \right) + \frac{1}{r} \frac{\partial}{\partial r} \left(r \Gamma_k \frac{\partial k}{\partial r} \right) + S^k \tag{16}$$

specific dissipation rate:

$$\frac{\partial}{\partial z}(\rho u \omega) + \frac{1}{r} \frac{\partial}{\partial r}(r \rho v \omega) = \frac{\partial}{\partial z} \left(\Gamma_\omega \frac{\partial \omega}{\partial z} \right) + \frac{1}{r} \frac{\partial}{\partial r} \left(r \Gamma_\omega \frac{\partial \omega}{\partial r} \right) + S^\omega \tag{17}$$

The turbulent viscosity for this model is defined by

$$\mu_t = \frac{\rho k}{\omega} \tag{18}$$

The exchange coefficients that affect the equations for k and ω in this model can be expressed as follows;

$$\Gamma_k = \mu + \frac{\mu_t}{\sigma_k} \quad (19)$$

$$\Gamma_\omega = \mu + \frac{\mu_t}{\sigma_\omega} \quad (20)$$

For this situation, the turbulent Prandtl/Schmidt numbers are $\sigma_k = \sigma_\omega = 2.0$. S^k and S^ω act as source terms for k and ω . Following expressions are providing them

$$S^k = \mu_t \left[2 \left\{ \left(\frac{\partial u}{\partial z} \right)^2 + \left(\frac{\partial v}{\partial r} \right)^2 + \left(\frac{v}{r} \right)^2 \right\} + \left\{ \frac{\partial v}{\partial z} + \frac{\partial u}{\partial r} \right\}^2 \right] - \beta^* \rho k \omega \quad (21)$$

$$S^\omega = \frac{\omega}{k} \mu_t \left[\left\{ \left(\frac{\partial u}{\partial z} \right)^2 + \left(\frac{\partial v}{\partial r} \right)^2 + \left(\frac{v}{r} \right)^2 \right\} + \left\{ \frac{\partial v}{\partial z} + \frac{\partial u}{\partial r} \right\}^2 \right] - \beta \rho \omega^2 \quad (22)$$

Constant are employed with standard values: $\beta^* = 0.09$ and $\beta = 0.072$.

Flow Structure and Boundary Conditions

Figure 1 illustrates a delineative view of the computational domain and twin jets configuration, providing details on the major dimensions, prescribed boundary conditions and the flow field. Two dominant main jet flows are expelled upward from nozzles with a diameter of $D=25$ mm and a velocity of U_0 , which in turn entrain the surrounding flow into the computational domain. At a distance of H from the nozzles, the twin jets will collide perpendicularly with a plate, causing the fluid flow direction to expand into the surrounding area. The distance between the two jet nozzles is represented by L . Impingement twin jet flows may be separated into five different flow regions: (1) the free jet, (2) combined wall jet, (3) jet impingement, (4) lower wall jet and (5) downwash fountain regions. At a distance far from the target impingement plate, referred to as the free jet region, the flow is primarily affected by axial velocity and relatively unaffected by impingement. In the unified wall jet zone, the ascendant velocity component exhibits a radial pattern, causing the boundary layer to thicken as it extends outward. Notably, the impingement zone of the twin jets, situated between free and wall jet zones, experiences significant alterations in the flow direction. The target impingement plate has two distinct stagnation points, both of which are located along the axis of the nozzles. At the midpoint between the twin jets, the secondary stagnation point coincides with the primary stagnation points along the direction of the nozzle axes. This center point location is where the flow is relatively stagnant, and the primary stagnation points align with the nozzle axes. Near the midpoint of the two jets, there exists a region known as the lower wall jet region. The region of downwash fountain is formed due to the encounter of the two individual jets as they impinge on the target surface.

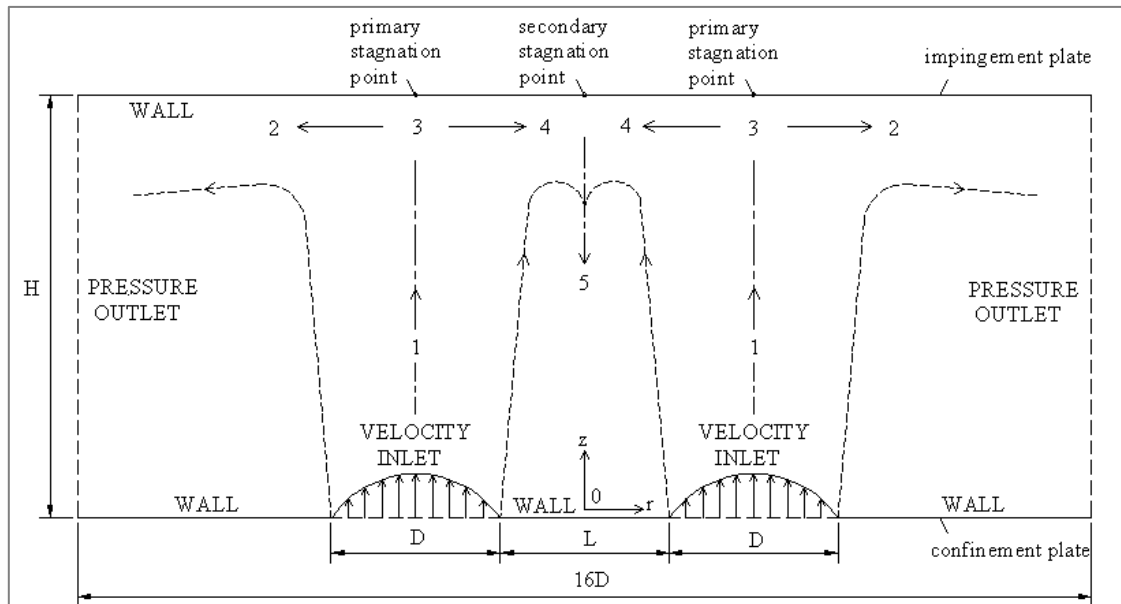


Figure 1. An illustration depicting the computational domain and twin jet configuration

The x-directional computational domain is approximately 16 times the nozzle diameter ($16D$) in length. To preserve both geometric and physical symmetry, numerical solution was performed only for the flow structure and field within the half domain. The computational domain was bounded by several specified boundary conditions. The target impingement plate was considered to have a constant temperature of $T_w = 323$ K and an isothermal wall condition was applied. Assuming that the confinement plate temperature was equal to the jet exit temperature, T_j was kept constant at 300 K. No-slip conditions were enforced on all walls, while the average velocity and turbulence profiles recorded at the outlet of the nozzles were employed as the velocity input parameters of the calculation domain. At the outlet planes, pressure outlet boundary conditions were deemed.

Numerical Solution Process

An implicit formulation with a segregated solver was used for solving the governing equations, employing a finite volume discretization method through the FLUENT 6.3.26 software. Central difference scheme used for approximating diffusion terms in the equations for the 2D simulations while second-order upwinding was employed for the convective terms. To establish a connection between the pressure and velocity fields, the SIMPLEC string was employed, which includes a face flux correction using modified equations. By utilizing a modified correction equation, the convergence rate is increased during the SIMPLEC procedure. To solve the pressure field, a conventional discretization method was employed. Other variables such as turbulent kinetic energy, momentum, rate of dissipation in turbulence and energy equation were solved using a second order discretization technique. High degree of accuracy particularly for complex flows involving separation is presenting by second order discretization scheme. One of the wall functions is enhancement wall treatment was employed to ensure reasonably accurate predictions. To ensure convergence, a residuals convergence criterion of 1×10^{-6} was applied to all

dependent variables and the sensitivity of grid distributions and numbers were tested for each case to procure the attainment of results independency from grid structure. Figure 2 displays the influence of the mesh density. The mesh was fine-tuned for every L/D and H/D value until negligible differences were observed and a finer computational grid with about 6000 cells in the whole computational domain was considered adequate. The estimation for the total discretization uncertainty was below 5%.

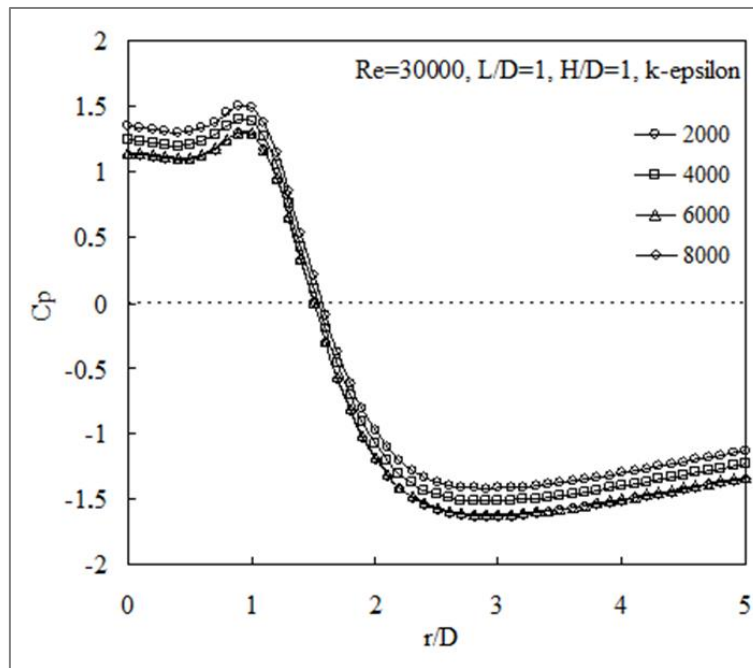


Figure 2. Influence of the mesh density

Experimental Study

The experimental apparatus schematized in Figure 3 and used for flow visualization and measurements consisted of a TE.88/3961 serial number system from Plint and Partners Ltd. The system was equipped with sensors to measure axial mean velocity, surface pressure and turbulence. Twin nozzles mounted vertically to a target impingement plate and a visualization system was employed to represent the flow of air exiting. The air was then directed to impinge on a flat plate mounted vertically to the jet axes in several distances from the confinement plate. The regulated supply air via a valve and was provided by a radial blower located under the main plate. To achieve a consistent flow towards the nozzles, a gauze screen was installed in the plenum chamber where the fan was connected. The nozzles had a diameter of 25 mm and a length of 50 mm, with slightly rounded inlets. Constructed from plexiglass, the impingement and confinement plates had a thickness of 5 mm and a diameter of 400 mm.

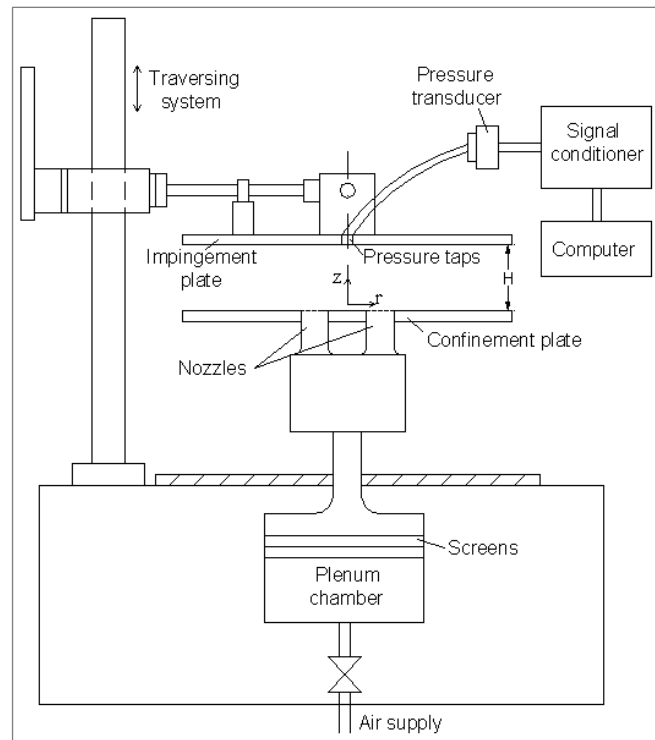


Figure 3. Schematic of the experimental apparatus

The smoke-wire technique [45, 46] was utilized to help visualize the flow structure and field. A stainless-steel wire with a diameter of 0.2 mm is placed opposite the nozzle outlet. Paraffin oil was used to coating the smoke wire and then DC current was applied to heat it by the Joule effect. The visualized flow pattern was successively photographed with a camcorder. Since this technique is also limited to low Reynolds numbers, flow visualization was executed at $Re=4800$. Visualization of flow behavior is very difficult at high Reynolds numbers. The hot wire anemometer TSI IFA-100 was used for one dimensional measurement of average velocity and turbulence in combination with a TSI 1220-20 hot film single probe. The data acquisition system interfaced with the hot-wire anemometer was used to collect 4096 samples at a rate of 1024 samples per second. A computer was used for data analysis. During the acquisition process, a filter with a cutoff frequency of 300 Hz was utilized to apply a low-pass effect on the data. At a Reynolds number of 30000 and $L/D=1$ and $H/D=1$, measurements of average velocity and turbulence were conducted. The tests were carried out at jet outlet velocities of up to 30 m/s, which ensured that compressibility effects remained neglect able. The Reynolds number was dependent on the diameter (D) of nozzle and the measured outlet velocity (U_o) of nozzle, which was determined using hot-wire anemometry. Turbulence intensity was kept below 1.5% even when testing jet velocities of 18, 24, and 30 m/s. A traversing unit, which had an accuracy of 0.1 mm, was employed to move the target impingement plate with respect to the jets in order to acquire pressure distributions on the jet impingement side of target surface. To measure surface pressure, a Setra-239 pressure transducer was utilized. Pressure sensors were installed on both the impinging and confining surfaces. The taps were then connected to a scanivalve through PVC tubing with an inner diameter of 1.6 mm and

a length of 600 mm. Sampling at each point was performed for 16 seconds. The signals captured by the transducer were digitally sampled at a rate of 1000 Hz, while being low pass filtered at 300 Hz. Estimates of measurement uncertainty indicated that axial velocity measurements were less than $\pm 3\%$ uncertain, while turbulence velocity measurements in the vertical direction were uncertain by $\pm 4\%$. The experimental outcomes were repeatable within the estimated uncertainty range of $\pm 2\%$ for the pressure measurements conducted on the target impingement plate and confinement surfaces.

Results and Discussions

In order to examine the confined impinging twin jets, numerical and experimental investigations were conducted at Reynolds numbers between 30000-50000, spacings of jet-to-jet (L/D) ranging from 0.5-2, and spacings of nozzle to target impingement plate (H/D) ranging from 0.5-2. Two turbulence models were utilized in the simulations, Standard $k-\omega$ and Realizable $k-\epsilon$, respectively.

Flow Structure

Figure 4 displays flow field images obtained using two turbulence models, while Figure 5 shows flow visualization photographs for H/D values of 1 and 2 at $L/D=1$. Numerical streamline images are obtained at $Re=30000$. Figure 4a shows the streamlines of the calculated velocity fields at $H/D=1$ and $L/D=1$ with Realizable $k-\epsilon$ turbulence model. The impinging jets result in the formation of two wall jets that spread radially at the impingement surface. As a result of the collision between the two jets, a downwash fountain flow is formed between them. Upon exiting the nozzle, each jet creates a negative pressure, which draws fluid from the surroundings and generates a vortex at the periphery of the jet. The peripheral vortices are then compressed between the jets and the downwash fountain flow. Streamlines calculated with Standard $k-\omega$ turbulence model exhibit an alike character with the Realizable $k-\epsilon$ model (Figure 4b). The photograph obtained from flow visualization study performed at $Re=4800$, $H/D=1$ and $L/D=1$ is shown in Figure 4c.

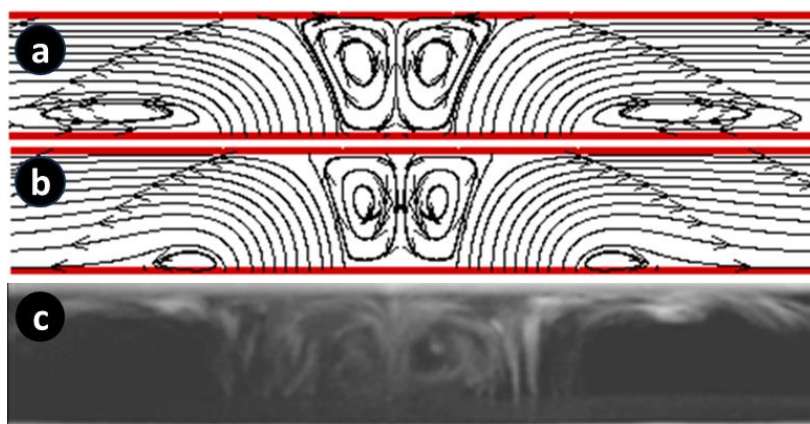


Figure 4. Visuals of the $H/D=1$ and $L/D=1$ confined impinging twin jet configuration. a) Streamline pattern derived using the Realizable $k-\epsilon$ turbulence model for $Re=30000$, b) Streamline pattern derived using the Standard $k-\omega$ turbulence model for $Re=30000$, c) Flow visualization image obtained with smoke-wire technique at $Re=4800$

Despite the difficulty in visualizing flow behavior at high Reynolds numbers, the presence of two counter rotating vortices between the nozzles is clearly evident. The downwash fountain flow interacts with the nozzle mainstream to produce low-pressure recirculation zones.

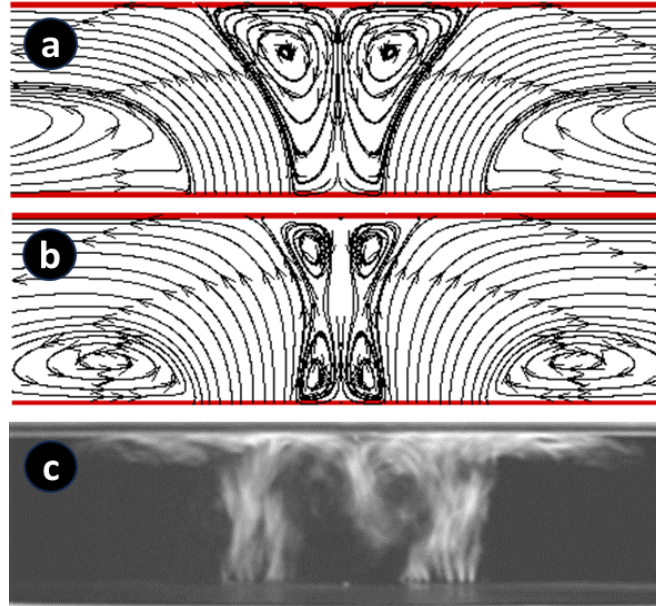


Figure 5. Visuals of the $H/D=2$ and $L/D=1$ confined impinging twin jet configuration. a). Streamline pattern derived using the Realizable $k-\epsilon$ turbulence model for $Re=30000$, b). Streamline pattern derived using the Standard $k-\omega$ turbulence model for $Re=30000$, c). Flow visualization image obtained with smoke-wire technique at $Re=4800$

Streamline plots are given at $H/D=2$ and $L/D=1$ for Realizable $k-\epsilon$ and Standard $k-\omega$ turbulence models in Figures 5a and 5b respectively. The size of the vortices is affected by the H/D ratio. The effect of the confinement plate on the counter rotating vortices close the target impingement plate is less pronounced, as shown in Figure 5c. For lowly spacings of nozzle to target impingement plate, the thickening wall jet pushes the peripheral vortex around each jet towards the confinement plate. The streamlines exhibit a toroidal recirculation zone, which increases in size and distance from the jet axis as H/D increases. The flow images obtained through numerical solutions match well with the flow visualizations captured in photographs. Calculation and measurement of axial velocity profiles and turbulence intensity behavior were conducted throughout the center lines of both jets. The distributions obtained for various nozzle-target impingement plate spacings at Reynolds number of 30000 and L/D ratio of 1 are displayed in Figures 6a and 6b. The turbulence intensity and axial velocity profiles have been normalized with nozzle exit velocity, U_0 and distancing of nozzle to target impingement plate, H , respectively. The results presented are for a single jet as the turbulence intensity and axial velocity profiles for both jets are similar. Figure 6a displays the measured and calculated axial velocity profiles throughout the center line of jet for $Re = 30000$ and $L/D=1$. The flow is decelerated and deflected due to the target impingement plate. The mean velocity in the axial direction decreases quickly after leaving the nozzle. As the distance between nozzle and target impingement plate increases, the effect of the impingement surface on the jet

decreases. The numerical results match the experimental data. The turbulence intensity changes throughout the jet centerline for the same conditions are demonstrated in Figure 6b. As the jet approaches the impingement surface, turbulence levels increase along the centerline. After the flow becomes fully developed, the turbulence intensity close the plate drops rapidly. Experimental data for $H/D=1$ shows higher turbulence intensity than the computed results for the same spacing. The observations made in Figures 4 and 5 are in agreement with these findings.

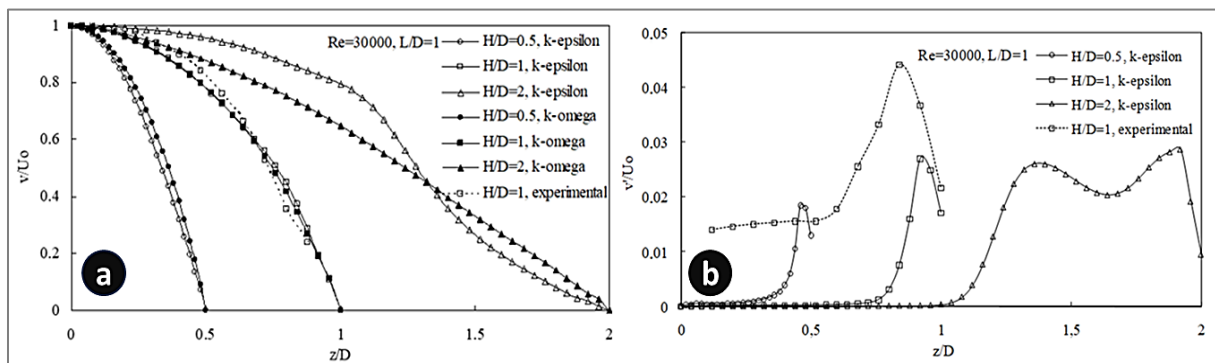


Figure 6. Axial velocity behavior on the jet midline at $Re=30000$ with $L/D=1$. a) average velocity, b) turbulence intensity

Figure 7a and 7b show the impact of nozzle to target impingement plate spacing (H/D) on local pressure distributions at $L/D=1$ and $Re=30000$, as calculated by the Realizable $k-\epsilon$ and Standard $k-\omega$ turbulence models respectively. The pressure distribution along the section between the center point of the jets and one edge of the plates is depicted in the plots. The plots reveal that region of sub-atmospheric pressure exist on the target impingement plate for all spacings of nozzle to target impingement plate examined. The secondary stagnation points, which indicate the midpoint between two jets, occur at $r/D=0$. Local pressure starts to slightly decrease from the secondary stagnation point for $H/D=0.5$ as the radial distance (r/D) increases, reaching a minimum value at $r/D\sim 0.7$, beyond which it starts to decrease again until it reaches the region of sub-atmospheric pressure where it hits a negative minimum value, and then increases towards the atmospheric value. As the distance between the nozzle and target impingement plate increases, the velocity of the fluid decreases as a result of the jet spreading out. Consequently, the point at which the pressure becomes sub-ambient shifts towards a bigger radial distance. As the ratio of H/D increases, the intensity of the sub-ambient region weakens. Additionally, the pressure gradient within this area alternates between negative and positive values (Figure 7a). As was discovered in Obot and Trabold's [47] study of impinging air jets, the flow separates from the surface due to the positive pressure gradient. As the H/D ratio increases, the maximum values at the primary stagnation points shift towards larger radial distances and decrease in magnitude. For instance, for $H/D=1$, the maximum occurs at $r/D\sim 0.9$, while for $H/D=2$, it occurs at $r/D\sim 1.45$. Jet spreading, which results in a decrease in kinetic energy at the jet center, is the cause of this effect as reported by Abdel-Fattah [18]. At $H/D=2$, the minimum values close the secondary stagnation point are no longer present. Figure 7b depicts that the local pressure distributions obtained with the Realizable $k-\epsilon$ model exhibit similar behavior to those

acquired with the Standard $k-\omega$ model for the similar parameters. However, the pressure coefficient values obtained with the Standard $k-\omega$ model are higher.

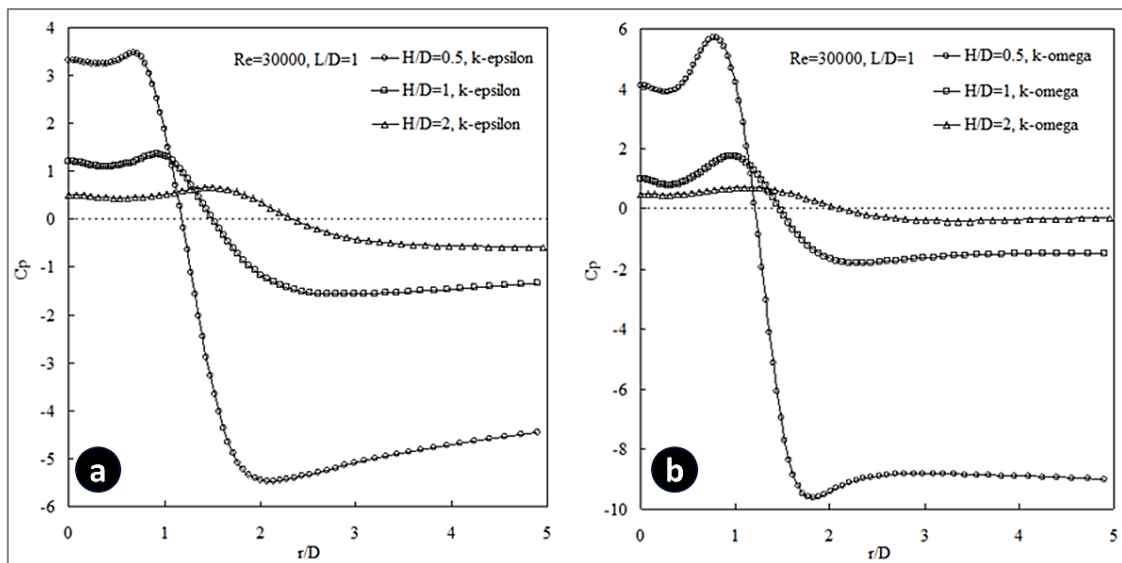


Figure 7. The relationship between nozzle to target impingement plate spacing and pressure distributions for $Re=30000$ at $L/D=1$. a) Realizable $k-\epsilon$ turbulence model b) Standard $k-\omega$ turbulence model

The Realizable $k-\epsilon$ turbulence model was utilized to investigate the effect of distance between two jets (L/D) on the local pressure distributions on the target impingement surface at $Re=30000$ and $H/D=1$, as shown in Figure 8. The figure illustrates that as increases on the spacing of jets, shifting the primary stagnation point to a larger radial distance. This is because the combination of the flow from the two jets occurs later with increasing L/D , resulting in a decrease in flow intensity [18].

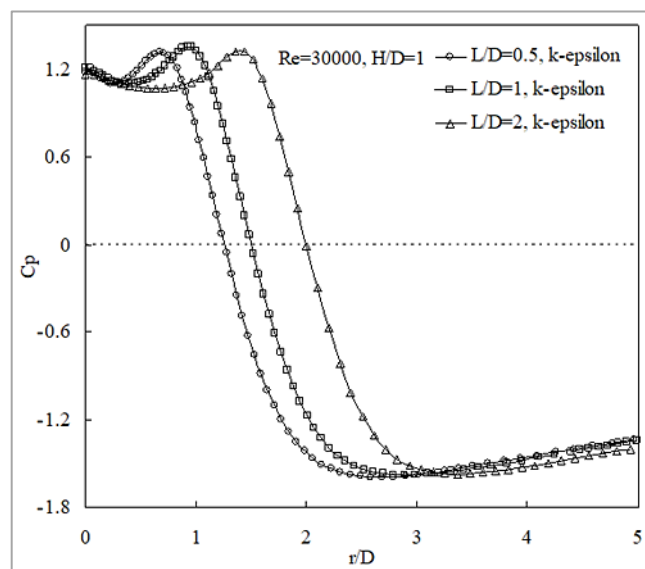


Figure 8. The relationship between jet-to-jet spacing and pressure distributions computed with the Realizable $k-\epsilon$ turbulence model for $Re=30000$ at $H/D=1$

On the target impingement plate, the surface pressure distributions are significantly impressed by the interplay of the two air jets. In other words, the figures show that the pressure coefficients on the

impingement surface are not affected by the Reynolds number, but are mightily dependent on the nozzle to target impingement plate spacings. The impingement surface exhibits a decrease in pressure as the flow accelerates, while the points of maximum pressure align with the stagnation points where the velocity is zero. This behavior is in line with the principles of global continuity. The experimental measurements indicate the existence of a region of sub-atmospheric pressure on the target impingement plate surface for nozzle to target impingement plate spacing up to 1, whereas numerical results reveal its presence for all nozzle to target impingement plate spacings studied. The deductive power of the sub-atmospheric zones increases as the nozzle to target impingement plate spacing decreases, resulting in a more pronounced effect. The numerically obtained pressure coefficients at the stagnating points are bigger than the experimental results measured at the same points for $H/D=0.5$ and 1 (Figures 9a and b). But for $H/D=2$, experimentally gathered pressure coefficients at the stagnation points are higher than the numerical results (Figure 9c). Compared to the experimentally obtained sub-atmospheric regions, greater sub-atmospheric regions are observed for both turbulence models. The evaluation of performance for both turbulence models indicates that the Realizable $k-\epsilon$ model displays preferable harmony with experimental results for H/D ratios of 0.5 and 1, while the Standard $k-\omega$ model is more successful at H/D ratio of 2.

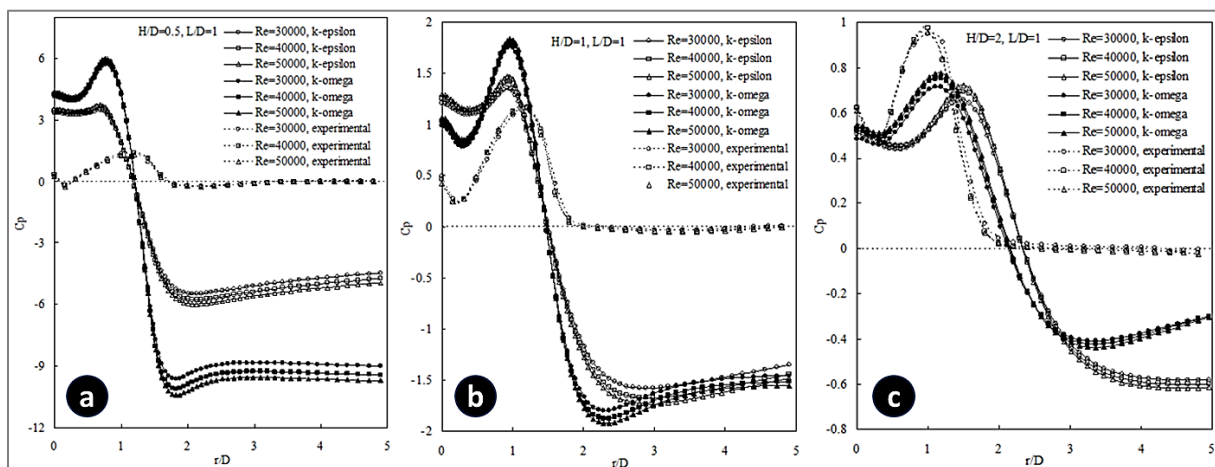


Figure 9. The influence of Reynolds number on the pressure distributions at $L/D=1$. a) $H/D=0.5$, b) $H/D=1$, c) $H/D=2$

It can be figured out from Figures 9a-c that as H/D increases, the closeness between the experimental and numerical outcomes increases as the simulation advances. The statement suggests that there are discrepancies between the computed and measured results, which are caused by the limitations of the turbulence models employed in the study. The models used may not be able to accurately capture the behavior of strongly curved flows. Additionally, the study is limited to 2D calculations, which may not fully reflect the 3D nature of the flow. The possibility of disparities arising between the computed and observed results cannot be ruled out.

Heat Transfer

In order to compare the impact of nozzle to target impingement plate spacing (H/D) on the target impingement plate's Nusselt number distributions at $Re=30000$ and $L/D=1$, we observe Figure 10a and Figure 10b, respectively, for Realizable $k-\epsilon$ and Standard $k-\omega$ turbulence models. The computation of the local Nusselt number involved the application of the formula $Nu = h \cdot D/k_a$, where $h = q / (T_w - T_j)$ stands for the coefficient of convective heat transfer, and T_j and T_w refer to the jet exit and impingement wall temperatures, respectively. The figures demonstrate that the Nusselt number distributions are extremely impressed by the distance between nozzle and target impingement plate. A decrease in the nozzle to target impingement plate distance causes a rise in both the primary stagnation Nusselt numbers and heat transfer ratios. For nozzle to target impingement plate spacings that are closer, the primary stagnation Nusselt number exhibits a higher rate of change. Aldabbagh and Sezai [14] have also reported similar findings. When the distance between nozzle and target impingement plate is reduced, the interaction zone between the two jets experiences a stronger interference. Nusselt numbers at the midpoint between the two jets exhibit very low values for all studied H/D spacings. Dong et al. [21] attribute this to the fact that the high-temperature reaction zone becomes detached from the target impingement plate. Figure 10a shows that the computed Nusselt profiles using the Realizable $k-\epsilon$ turbulence model exhibit three peaks. When H/D is equal to 0.5, the first peak appears at $r/D \approx 0.6$, followed by the second peak at $r/D \approx 1.2$ and the third peak at $r/D \approx 2.3$. The observed peaks in the Nusselt number data are associated with the transition of the flow from a laminar to a turbulent state in the wall jet region. This transition leads to an increase in turbulence levels near the wall, which explains the rise in the Nusselt number. Second peak takes higher values than the two other peaks. With an increase in H/D spacings, the figured out Nusselt number peaks on the impingement surface decrease and shift to larger radial distances, occurring every three peaks. The increase in primary vortex size with an increase in H/D , as shown in Figure 5, is the reason behind this phenomenon. The positions of minimum values of Nu move toward the center of target impingement plate as H/D decreases. As the H/D ratio decreases, the primary vortex size also decreases, resulting in steeper slopes of the Nu curves. This is due to the reduction in the size of regions with adverse pressure gradients as H/D decreases. The radial locations of the minimum Nu values between the first and second peaks are similar to the radial locations of the primary stagnation points of the pressure coefficients shown in Figure 7a. Moreover, the regions where the second peaks in Nusselt distributions occur correspond to sub-atmospheric local pressures on the target impingement plate.

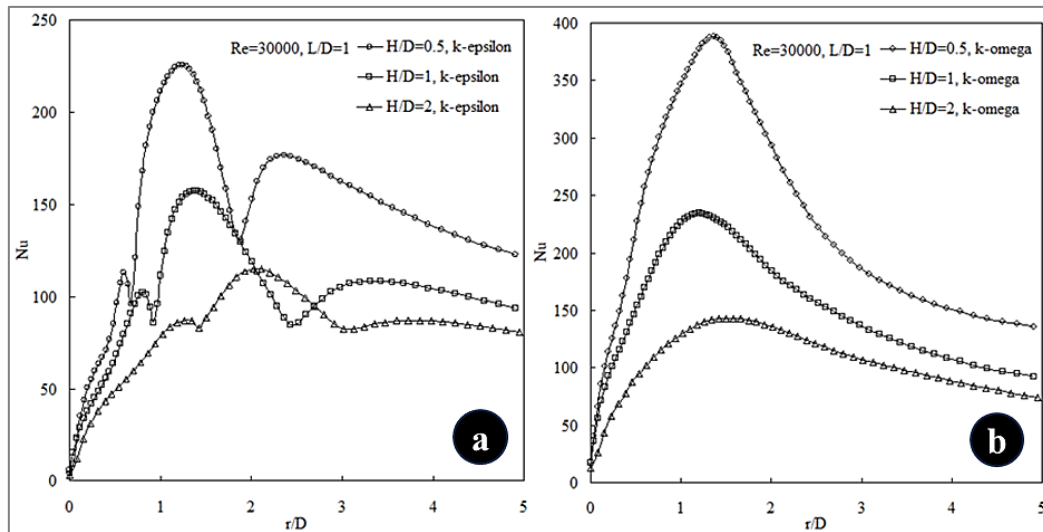


Figure 10. The relationship between nozzle to target impingement plate spacing and local Nusselt number distributions for $Re=30000$ at $L/D=1$. a) Realizable $k-\epsilon$ turbulence model, b) Standard $k-\omega$ turbulence model

For every studied H/D spacing, only one peak in the Nusselt number distribution on the impingement surface is computed by the Standard $k-\omega$ turbulence model (Figure 10b). Dong et al. [21] observed that the heat transfer distributions of twin jets obtained from the Realizable $k-\epsilon$ model are more consistent with experimental data than those obtained from another turbulence model. Figure 11 demonstrates the impact of the distance between twin jets (L/D) on the radial distribution of the local Nusselt number on the target impingement plate at $Re=30000$ and $H/D=1$.

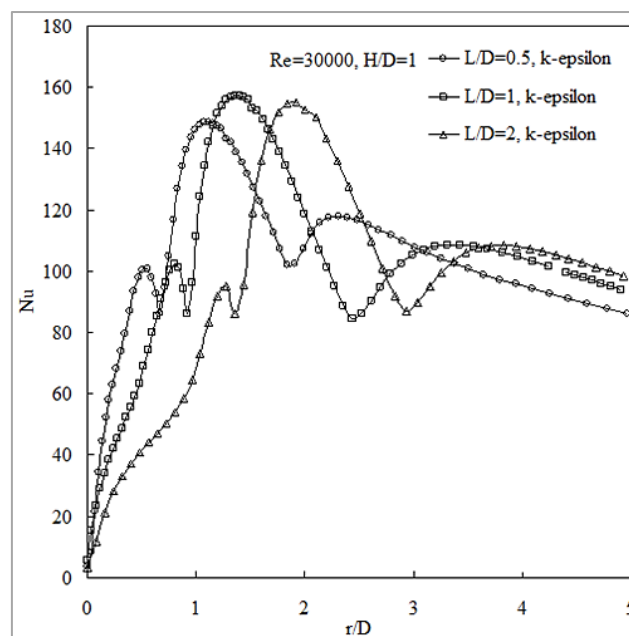


Figure 11. The relationship between jet-to-jet spacing and local Nusselt number distributions for $Re=30000$ at $H/D=1$ using the Realizable $k-\epsilon$ turbulence model.

These results are predicted using the Realizable $k-\epsilon$ turbulence model. Observations show that the magnitude of the Nusselt number is unaffected by the distance between twin jets, but the Nusselt number peaks shift towards the radial direction. Regardless of the L/D value, a region with lower heat transfer

rate occurs at the midpoint between the double jets. This suggests that the heat transfer to the plate is hindered due to the interference between the double jets. Figure 12 illustrates the influence of Reynolds number on the heat transfer distributions at $H/D=1$ and $L/D=1$, as calculated using the Realizable $k-\varepsilon$ and Standard $k-\omega$ turbulence models. The figure presents a comparison of the two turbulence models results under different Reynolds number conditions. The observed increase in local Nusselt numbers with a rise in Reynolds number results in improved convective heat transfer. The effect is attributed to the formation of the downwash fountain, which occurs as a result of the colliding wall jets after impingement. The downwash fountain's presence contributes significantly to the observed phenomenon. The Nusselt profiles exhibit a similar trend for different Reynolds numbers of 30000, 40000, and 50000. Three peaks are evident in the Realizable $k-\varepsilon$ model, with the second peak being the largest of the three. Cooper et al [48] stated that the secondary peak in the Nusselt number is due to an increase in the level of turbulence near the wall. The location of the peak predicted by the Standard $k-\omega$ model differs from the multiple peaks predicted by the Realizable $k-\varepsilon$ model. Radial locations of Nusselt peaks are independent of the Reynolds number. The Realizable $k-\varepsilon$ model predicts local Nusselt number magnitudes that are lower than those predicted by the Standard $k-\omega$ model. The suitability of the Realizable $k-\varepsilon$ model for modeling the flow field with a strong adverse pressure gradient, in contrast to the Standard $k-\omega$ model, is the reason for the observed discrepancy in the predicted Nusselt number peaks.

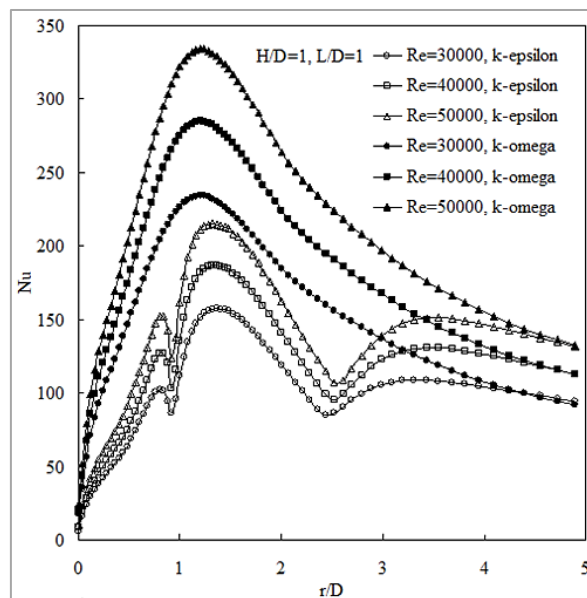


Figure 12. The relationship between Reynolds number and local Nusselt number distributions using Realizable $k-\varepsilon$ and Standard $k-\omega$ turbulence models for $H/D=1$ at $L/D=1$

Conclusion

Experiments and numerical simulations were carried out in present study to investigate the flow structures and fields of the confined twin impinging jet, as well as to determine its heat transfer performance and properties, encompassing Reynolds numbers up to 50000 and different spacings of

nozzle to target impingement plate and jet-to-jet. The collision of the jets close the impingement plate leads to the formation of two counter rotating circular vortices and a downwash fountain flow between the jets. The interplay between the primary jet and the downwash flow creates low-pressure regions, leading to the formation of recirculation zones. These zones are a consequence of the interplay between the two flow components. The flow is decelerated and deflected by the impinging plate. Both numerical and experimental pressure distributions on the impingement surface show a dependence on the distance between nozzle to target impingement plate and twin jets, while being independent of Reynolds number. Additionally, the Standard $k-\omega$ turbulence model exhibits higher pressure coefficients in comparison to the Realizable $k-\varepsilon$ turbulence model. These findings highlight the disparities between the two turbulence models' predictions in terms of pressure coefficients. Regions of sub-atmospheric pressure on the impingement surface for spacing up to 1 are observed at the experimental measurements, while they exist at all studied nozzle to target impingement plate spacings for numerical results. The numerically predicted pressure coefficients are greater than the experimentally obtained pressure coefficients. Nusselt number distributions predicted with two turbulence models depend on Reynolds numbers, distances between twin jets and nozzle to target impingement plate. Nusselt number distributions obtained Realizable $k-\varepsilon$ model have different form from Standard $k-\omega$ model results. While Standard $k-\omega$ model exhibits only one peak, Realizable $k-\varepsilon$ model shows three peaks in the Nusselt profiles. Based on the Realizable $k-\varepsilon$ model, the pressure coefficients on the impingement plate are sub-atmospheric at the radial distances where the second peaks in Nusselt numbers are observed. This relation demonstrates the correlation between sub-atmospheric regions in pressure distribution and heat transfer coefficient peaks on the impingement surfaces. The study's results indicate that the Realizable $k-\varepsilon$ turbulence model is superior to the Standard $k-\omega$ turbulence model in terms of predicting flow fields and structures as well as heat transfer distributions. The inconsistencies in the experimental and numerical findings may stem from the narrow coverage of the turbulence models utilized, in conjunction with a 2D computational domain.

Acknowledgments We acknowledge the Karadeniz Technical University Department of Mechanical Engineering for providing the test equipment and programme.

Funding/Financial Disclosure The authors have no received any financial support for the research, authorship, or publication of this study.

Ethics Committee Approval and Permissions The study does not require ethics committee permission or any special permission.

Conflict of Interests The authors declare no conflict of interest.

Authors Contribution Yücel ÖZMEN contributed 70% to the article and performed, analysed and interpreted the experiments. Haluk KELEŞ contributed 30% to the article, prepared the graphs and wrote the article

References

- [1] Barata, J. M. M., Durao, D. F. G. & Heitor, M. V. (1991). Impingement of single and twin turbulent jets through a cross-flow. *AIAA Journal*, 29, 595-602. <https://doi.org/10.2514/3.10626>
- [2] Chuang, S. H., Chen, M. H., Lii, S. W. & Tai, F. M. (1992). Numerical simulation of twin-jet impingement on a flat plate coupled with cross-flow. *International Journal for Numerical Methods in Fluids*, 14, 459-475. <https://doi.org/10.1002/flid.1650140406>
- [3] Chuang, S. H. & Nieh, T. J. (2000). Numerical simulation and analysis of three-dimensional turbulent impinging square twin jet flow field with no-cross flow. *International Journal of Numerical Methods in Fluids*, 33, 475-498. [https://doi.org/10.1002/1097-0363\(20000630\)33:4<475::AID-FLD16>3.0.CO;2-Q](https://doi.org/10.1002/1097-0363(20000630)33:4<475::AID-FLD16>3.0.CO;2-Q)
- [4] Polat, S., Huang, B., Mujumdar, A. S. & Douglas, W. J. (1989). Numerical flow and heat transfer under impinging jets. *Annual Review of Numerical Fluid Mechanics and Heat Transfer*, 2, 157-197. <https://doi.org/10.1615/AnnualRevHeatTransfer.v2.60>
- [5] Shi, Y. L., Ray, M. B. & Mujumdar, A. S. (2002). Computational study of impingement heat transfer under a turbulent slot jet. *Industrial & Engineering Chemistry Research*, 41, 4643-4651. <https://doi.org/10.1021/ie020120a>
- [6] Seyedein, S. H., Hasan, M. & Mujumdar, A. S. (1995). Turbulent flow and heat transfer from confined multiple impinging slot jets. *Numerical Heat Transfer*, 18, 35-51. <https://doi.org/10.1080/10407789508913687>
- [7] Dianat, M., Fairweather, M. & Jones, W. P. (1996). Prediction of axisymmetric and two dimensional impinging turbulent jets. *International Journal of Heat and Fluid Flow*, 17, 530-538. [https://doi.org/10.1016/S0142-727X\(96\)00076-8](https://doi.org/10.1016/S0142-727X(96)00076-8)
- [8] Fernandez, J. A., Elicer-Cortes, J. C., Valencia, A., Pavagean, M. & Gupta, S. (2007). Comparison of low cost two equation turbulence models for prediction flow dynamics in twin jet devices. *International Communications in Heat and Mass Transfer*, 34, 570-578. <https://doi.org/10.1016/j.icheatmasstransfer.2007.02.011>
- [9] Miao, J. M., Wu, C. Y. & Chen, P. H. (2009). Numerical investigation of confined multiple jet impingement cooling over a flat plate at different cross flow orientations. *Numerical Heat Transfer, Part A*, 55, 1019-1050. <https://doi.org/10.1080/10407780903014335>
- [10] Qiu, S., Xu, P., Jiang, Z. & Mujumdar, A. S. (2012). Numerical modeling of pulsed laminar opposed impinging jets. *Engineering Applications of Computational Fluid Mechanics*, 6(2), 195-202. <https://doi.org/10.1080/19942060.2012.11015414>
- [11] Attalla, M & Specht, E. (2009). Heat transfer characteristics from in-line arrays of free impinging jets. *Heat and Mass Transfer*, 45, 537-543. <https://doi.org/10.1007/s00231-008-0452-y>
- [12] Aldabbagh, L. B. Y. & Mohamad, A. A. (2007). Effect of jet-to-plate spacing in laminar array jets impinging. *Heat and Mass Transfer*, (43), 265-273. <https://doi.org/10.1007/s00231-006-0109-7>

- [13] Dagtekin, I. & Oztop, H.F. (2008). Heat transfer due to double laminar slot jets impingement on to an isothermal wall within one side closed long duct. *International Communications in Heat and Mass Transfer*, 35, 65-75. <https://doi.org/10.1016/j.icheatmasstransfer.2007.05.013>
- [14] Aldabbagh, L. B. Y. & Sezai, I. (2002). Numerical simulation of three-dimensional laminar, square twin-jet impingement on a flat plate, flow structure and heat transfer. *Numerical Heat Transfer, Part A*, 41, 835-850. <https://doi.org/10.1080/10407780290059378>
- [15] Ho, C. M. & Hsiao, F. B. (1982, August 31 - September 3). *Evolution of coherent structure in a lip jet* [Conference presentation]. International Symposium on Structure of Complex Turbulent Shear Flow, Marseille, France 121-136. https://doi.org/10.1007/978-3-642-81991-9_13
- [16] Siclari, M. J., Hill, J. W. G. & Jenkins, R. C. (1981). Stagnation line and upwash formation of two impinging jets. *AIAA Journal*, 19, 1286-1293. <https://doi.org/10.2514/3.60062>
- [17] Tanaka, E. (1974). The interference of two dimensional parallel jets experiments on the combined flow of dual jets. *Bulletin ASME*, 17, 920-927. <https://doi.org/10.1299/JSME1958.17.920>
- [18] Abdel-Fattah, A. (2007). Numerical and experimental study of turbulent impinging twin jet flow. *Experimental Thermal and Fluid Science*, 31, 1060-1072. <https://doi.org/10.1016/j.expthermflusci.2006.11.006>
- [19] Mikhail, S., Morces, S. M., Absu-Ellail, M. M. M. & Ghaly, W. S. (1982). Numerical prediction of flow field and heat transfer from a row of laminar slot jets impinging on a flat plate. *Heat Transfer*, 3, 377-382.
- [20] Barata, J. M. M. (1996, November 18-20,). *Ground vortex formation with twin impinging jets* [Conference presentation]. International Powered Lift Conference, Florida, USA. <https://www.jstor.org/stable/44725610>
- [21] Dong, L. L., Leung, C. W. & Cheung, C. S. (2004). Heat transfer and wall pressure characteristics of a twin premixed butane/air flame jets. *International Journal of Heat and Mass Transfer*, 47, 489-500. <https://doi.org/10.1016/j.ijheatmasstransfer.2003.07.019>
- [22] Saad, N. R., Polat, S. & Douglas, W. J. M. (1992). Confined multiple impinging slot jets without crossflow effects. *Int J Heat Fluid Flow*, 13, 2-14. [https://doi.org/10.1016/0142-727X\(92\)90054-D](https://doi.org/10.1016/0142-727X(92)90054-D)
- [23] Ozmen, Y. (2011). Confined impinging twin air jets at high Reynolds numbers. *Experimental Thermal and Fluid Science*, 35, 355-363. <https://doi.org/10.1016/j.expthermflusci.2010.10.006>
- [24] Buchlin, J. M. (2011). Convective heat transfer in impinging- gas- jet arrangements. *Journal of Applied Fluid Mechanics (JAFM)*, 4, 137-149. <https://doi.org/10.36884/jafm.4.02.11926>
- [25] Polat S., Huang B., Mujumdar A. S. & Douglas W. J. M. (1989). Numerical flow and heat transfer under impinging jets: A review. *Annual Review of Heat Transfer*, 2, 157-197. <https://doi.org/10.1615/AnnualRevHeatTransfer.v2.60>
- [26] Ozmen, Y. & Ipek, G. (2016). Investigation of flow structure and heat transfer characteristics in an array of impinging slot jets. *Heat and Mass Transfer*, 52, 773-787. <https://doi.org/10.1007/s00231-015-1598-z>
- [27] Ozmen, Y. & Baydar, E. (2013). A numerical investigation on confined impinging array of air jets. *Journal of Thermal Science and Technology*, 33, 65-74.

- [28] Afroz F. & Sharif, M. A. R. (2013). Numerical study of heat transfer from an isothermally heated flat surface due to turbulent twin oblique confined slot-jet impingement. *International Journal of Thermal Sciences*, 74, 1-13. <https://doi.org/10.1016/j.ijthermalsci.2013.07.004>
- [29] Yousefi-Lafouraki, B., Ramiar, A. & Ranjbar, A. A. (2014). Laminar forced convection of a confined slot impinging jet in a converging channel. *International Journal of Thermal Sciences*, 77, 130-138. <https://doi.org/10.1016/j.ijthermalsci.2013.10.014>
- [30] Al-Rmah, M. A. & Mohamad, A. A. (2015). Simulation of multi-internal confined impinging jets using the lattice boltzmann method. *Applied Thermal Engineering*, 81, 288-296. <https://doi.org/10.1016/j.applthermaleng.2015.02.038>
- [31] Guoneng, L., Zhihua, X., Youqu, Z., Wenwen, G. & Cong D. (2016). Experimental study on convective heat transfer from a rectangular flat plate by multiple impinging jets in laminar cross flows. *International Journal of Thermal Sciences*, 108, 123-131. <https://doi.org/10.1016/j.ijthermalsci.2016.05.006>
- [32] Lam, P. A. K. & Prakash, K. A. (2017). A numerical investigation and design optimization of impingement cooling system with an array of air jets. *International Journal of Heat and Mass Transfer*, 108, 880–900. <https://doi.org/10.1016/j.ijheatmasstransfer.2016.12.017>
- [33] Paulraj, M. P., Byon, C., Vallati, A. & Parthasarathy, R. K. (2020). A numerical investigation of flow and heat transfer of laminar multiple slot jets impinging on multiple protruding heat sources. *Heat Transfer Engineering*, 41, 65-83. <https://doi.org/10.1080/01457632.2018.1513629>
- [34] Kaya, H. (2021). İkili çarpan jet ile soğutulan sıcak plakanın yüzey şeklinin ısı transferine etkisinin sayısal analizi. *Düzce Üniversitesi Bilim ve Teknoloji Dergisi*, 9, 152-163. <https://doi.org/10.29130/dubited.754908>
- [35] Martinez-Filguera, P., Portal-Porras, K., Fernandez-Gamiz, U., Zulueta, E. & Soriano, J. (2022). Experimental and numerical modeling of an air jet impingement system. *European Journal of Mechanics-B/Fluids*, 94, 228-245. <https://doi.org/10.1016/j.euromechflu.2022.03.005>
- [36] Demircan, T. & Türkoğlu, H. (2010). Çarpan osilasyonlu jetlerde osilasyon karakteristiklerinin ve çarpma mesafesinin akış ve ısı transferine etkilerinin sayısal olarak incelenmesi. *Gazi Üniversitesi Mühendislik Mimarlık Fakültesi Dergisi*, 25 (4), 895-904. <https://dergipark.org.tr/tr/pub/gazimmfd/issue/6686/88613>
- [37] Bolek, A. & Bayraktar, S. (2019). Flow and heat transfer investigation of a circular jet issuing on different types of surfaces. *Sādhanā* 44, 242. <https://doi.org/10.1007/s12046-019-1226-6>.
- [38] Çalışır, T., Başkaya, Ş., Çalışkan, S. & Kılıç, M. (2017). Çarpan akışkan jetleri kullanarak kanatçıklı yüzeyler üzerindeki akış alanının sayısal olarak incelenmesi. *Gazi Üniversitesi Mühendislik Mimarlık Fakültesi Dergisi*, 32 (1): 119-130. <https://doi.org/10.17341/gazimmfd.300601>.
- [39] Wang, S. J. & Mujumdar, A. S. (2005). A comparative study of five low Reynolds number k-ε models for impingement heat transfer. *Applied Thermal Engineering*, 25, 31-44. <https://doi.org/10.1016/j.applthermaleng.2004.06.001>
- [40] Park, T. H., Choi, H. G., Yoo, J. Y. & Kim, S. J. (2003). Streamline upwind numerical simulation of two-dimensional confined impinging slot jets. *International Journal of Heat and Mass Transfer*, 46, 251-262. [https://doi.org/10.1016/S0017-9310\(02\)00270-3](https://doi.org/10.1016/S0017-9310(02)00270-3)

- [41] Bentarzi, F., Mataoui, A. & Rebay, M. (2019). Effect of inclination of twin impinging turbulent jets on flow and heat transfer characteristics. *International Journal of Thermal Sciences*, 137, 490-499. <https://doi.org/10.1016/j.ijthermalsci.2018.12.021>
- [42] Youn, J. S., Choi, W. W. & Kim, S. M. (2021). Numerical investigation of jet array impingement cooling with effusion holes. *Applied Thermal Engineering*, 197, 117-147. <https://doi.org/10.1016/j.applthermaleng.2021.117347>
- [43] Singh, P. K., Renganathan, M., Yadav, H., Sahu, S. K., Upadhyay, P. K. & Agrawal, A. (2022). An experimental investigation of the flow-field and thermal characteristics of synthetic jet impingement with different waveforms. *International Journal of Heat and Mass Transfer*, 187, 122534. <https://doi.org/10.1016/j.ijheatmasstransfer.2022.122534>
- [44] Sharif, M. A. R. (2013). Heat transfer from an isothermally heated flat surface due to confined laminar twin oblique slot-jet impingement. *Journal of Thermal Science and Engineering Applications*, 7, 031001. <https://doi.org/10.1016/j.proeng.2013.03.158>
- [45] Cornaro, C., Fleischer, A. S. & Goldstein R. J. (1999). Flow visualization of a round jet impinging on cylindrical surfaces. *Experimental Thermal and Fluid Science*, 20, 66-78. [https://doi.org/10.1016/S0894-1777\(99\)00032-1](https://doi.org/10.1016/S0894-1777(99)00032-1)
- [46] Travnicek, Z. & Tesar, V. (2004). Annular impinging jet with recirculation zone expanded by acoustic excitation. *International Journal of Heat and Mass Transfer*, 47, 2329-2341. <https://doi.org/10.1016/j.ijheatmasstransfer.2003.10.032>
- [47] Obot, N. T. & Trabold, T. A. (1987). Impinging heat transfer within arrays of circular jets: Part 1-effects of minimum, intermediate and complete cross flow for small and large spacings. *Journal of Heat Transfer*, 109, 872-879. <https://doi.org/10.1115/1.3248197>
- [48] Cooper, D., Jackson, D. C., Launder, B. E. & Liao, G. X. (1993). Impinging jet studies for turbulence model assessment-I. Flow field experiments. *International Journal of Heat and Mass Transfer*, 36, 2675-2684. [https://doi.org/10.1016/S0017-9310\(05\)80204-2](https://doi.org/10.1016/S0017-9310(05)80204-2)